PERFORMANCE ANALYSIS OF A COAXIAL ROTOR SYSTEM IN HOVER: THREE POINTS OF VIEW

Jessica Yana* , **Omri Rand****
Graduate student,*Professor**
Technion - Israel Institute of Technology
yjessica@tx.technion.ac.il; omri@aerodyne.technion.ac.il;

Keywords: *coaxial rotor, aerodynamics, performance, vortex*

Abstract

The paper deals with the problem of the aerodynamic analysis of a coaxial rotor system in hover from three points of view: An analytic point of view; a computational point of view which is based on rigid wake model; and a computational point of view which is based on free wake model.

The analytical model includes also an optimization scheme for coaxial system. The three methods are compared and discussed along with correlation with various experiments.

1 General Introduction

A coaxial rotor system is an arrangement that contains two identical, or nearly identical, counter-rotating rotors along a common spin axis; i.e., coaxially. An important advantage of coaxial rotor configuration over the traditional single main rotor configuration is its improved efficiency and compact design. The efficiency improvement stems from the larger disc area and from the removal of the tail rotor, which consumes power, yet contributes little or nothing to the thrust. The resulting compact design improves maneuver performance, reduces airborne vulnerability, and conserves space in cramped landing areas, such as aircraft carrier flight decks. In addition, significant speed improvements are potentially achievable for coaxial rotorcraft, although at the cost of increased vibration level.

The present effort deals with the problem of the aerodynamic analysis of a coaxial rotor system in hover from three points of view which are founded on a common basis: An analytic point of view; a computational point of view which is based of rigid wakes; and a computational point of view which is based of free wakes. The common basis of this study is the Blade-Element Theory which in the general case is founded on a lookup table technique for the airfoils polars. Such approach allows physical insight to the performance analysis issues which are crucial for simulation and preliminary design.

In the analytical model, the upper rotor model takes into account the lower rotor induced velocity as an "equivalent climb speed" and the lower rotor model takes into account the upper rotor induced velocity in a similar, yet more complex way. The proposed analysis also includes a search for aerodynamically optimal coaxial rotor that eventually minimizes the total (induced and parasite) power. This search is founded on a calculus of variations theorem that exploits the Blade-Element Momentum Theory.

A relatively simple computational point of view is founded on a rigid (prescribed) wake for each rotor. Wake geometry and its parameters are obtained from experimentally and computationally collected data from the open literature. In this case, the mutual interaction between rotors is accounted for by the rigid wakes induced velocity distribution over both disks.

For the computational point of view with free

wakes, both wakes are determined by a time marching numerical scheme. Such modeling offers a higher level of fidelity for the aerodynamic analysis, although at considerably high computational cost. The model is capable of capturing the mutual interference of the wakes which leads to their geometry and strength characteristics and subsequently to the unique coaxial rotor system performance.

2 Analytical point of view

Fig. 1 shows a coaxial system of two concentric rotors with a clearance, h, that rotate in opposite directions. The rotors are not necessarily identical in all parameters including their radius, rotational speed, number of blades, chord and airfoil distribution, etc. (i.e. $R^U \neq R^L$ and $\Omega^U \neq \Omega^L$, $N_b^U \neq N_b^L$, $\tilde{c}^U(\tilde{r}) \neq \tilde{c}^L(\tilde{r})$ in the general case).

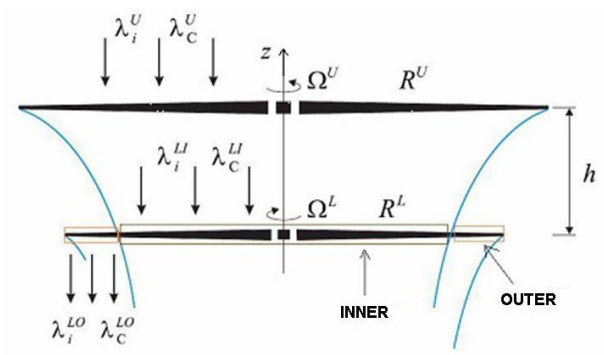

Fig. 1 Coaxial rotor system in hover

In this model, the upper rotor model takes into account the lower rotor induced velocity as an "equivalent climb speed" and similarly, the lower rotor model takes into account the upper rotor induced velocity as an "equivalent climb speed" as well. The present model is developed and presented in two parallel courses where the above described mutual influences are founded on uniform downwash distributions for the simplified course and on nonuniform downwash distributions for the second course.

2.1 The Mutual Interaction Between the Rotors

As indicated above, the upper rotor is submerged in the downwash that is induced by the lower rotor. This downwash is written as $k^{LU}\bar{\lambda}_i^L\frac{\zeta_R}{\zeta_\Omega}$ where k^{LU} is an influence coefficient and $\bar{\lambda}_i^L$ is the averaged nondimensional induced velocity over the lower rotor. In general, k^{LU} is a function of $\tilde{r}^U$ (radial station). Similarly, the inner part of the lower rotor is submerged in the downwash that is induced by the upper rotor and is written as $k^{UL}\bar{\lambda}_i^U\frac{\zeta_\Omega}{\zeta_R}$ where k^{UL} is an influence coefficient and $\bar{\lambda}_i^U$ is the averaged nondimensional induced velocity over the upper rotor. Clearly, k^{UL} is a function of $\tilde{r}^L$. Hence in the general case, the equivalent climb velocities over the upper and the lower rotors are:

$$\lambda_C^U(\tilde{r}) = k^{LU}(\tilde{r})\bar{\lambda}_i^L\frac{\zeta_R}{\zeta_\Omega}, \tag{1a}$$

$$\lambda_C^L(\tilde{r}) = k^{UL}(\tilde{r})\bar{\lambda}_i^U\frac{\zeta_\Omega}{\zeta_R} \tag{1b}$$

where

$$\zeta_R = \frac{R^L}{R^U}; \qquad \zeta_\Omega = \frac{\Omega^U}{\Omega^L}$$

Note that $\bar{\lambda}_i^L$ and $\bar{\lambda}_i^U$ are the averaged induced velocity over the *disc areas* and are therefore expressed as:

$$\bar{\lambda}_i^U = 2\int_0^1 \tilde{r}\lambda_i^U(\tilde{r})d\tilde{r}; \quad \bar{\lambda}_i^L = 2\int_0^1 \tilde{r}\lambda_i^L(\tilde{r})d\tilde{r}.$$

The simplified model: In the simplified model we assume that k^{LU} is constant, and k^{UL} is constant for $\tilde{r}^L < \tilde{r}_w^L$ and vanishes for $\tilde{r}_w^L < \tilde{r}^L < 1$. In such a case, $\lambda_i^U(\tilde{r})$ of the optimal design turns to be also constant. Similarly, $\lambda_i^L(\tilde{r})$ becomes constant for $\tilde{r}^L < \tilde{r}_w^L$ (and will be denoted λ_i^{LI} there), while it takes a value of different constant for $\tilde{r}_w^L < \tilde{r}^L < 1$ (and will be denoted λ_i^{LO} there). Hence, in such a case, the equivalent climb velocities are given by:

$$\lambda_C^U = \tag{2}$$

$$k^{LU}\left\{\left(\tilde{r}_w^L\right)^2\lambda_i^{LI} + \left[1-\left(\tilde{r}_w^L\right)^2\right]\lambda_i^{LO}\right\}\frac{\zeta_R}{\zeta_\Omega},$$

$$\lambda_C^{LI} = \left[k^{UL}\lambda_i^U\right]\frac{\zeta_\Omega}{\zeta_R}, \quad (3a)$$

$$\lambda_C^{LO} = 0. \quad (3b)$$

Estimation of the influence coefficients

The estimation of the averaged values of the influence coefficients $k^{UL}(\tilde{r}^L)$ and $k^{LU}(\tilde{r}^U)$ is based on the average induced velocity distribution below and above a single rotor and are subsequently given by:

$$k^{UL} = 1+\left(\frac{d}{\sqrt{1+d^2}}\right)^{\gamma_{UL}};\ k^{LU} = 1-\left(\frac{d}{\sqrt{1+d^2}}\right)^{\gamma_{LU}}$$

where $d = \left|{}^{h}/_{R}\right|$ and the estimation of the coefficients γ_{UL} and γ_{LU} has been obtained thanks to comparison with experimental data: $\gamma_{UL} = 0.6$ and $\gamma_{LU} = 0.3 \div 0.5$ (see Fig. 2).

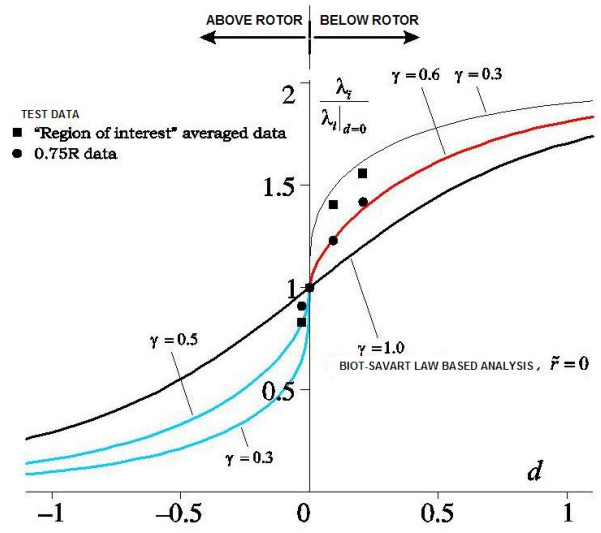

Fig. 2 Averaged induced velocity distribution below and above a single rotor.

Fig. 7 presents a free wake geometry of a single rotor. The wake contraction is clearly observed. The induced velocity of such a wake is not uniform in the general case. The resulting influence coefficients in such a case are expressed as:

$$k^{UL}(\tilde{r}^L) = \frac{\lambda^{*L}(\tilde{r}^L)}{\bar{\lambda}_i^U\frac{\zeta_\Omega}{\zeta_R}}; \qquad k^{LU}(\tilde{r}^U) = \frac{\lambda^{*U}(\tilde{r}^U)}{\bar{\lambda}_i^L\frac{\zeta_R}{\zeta_\Omega}}$$

where $\lambda^{*U}(\tilde{r}^U)$ and $\lambda^{*L}(\tilde{r}^L)$ are the time averaged values as functions of the radial stations.

2.2 The Proposed Optimal Coaxial System Analysis

The proposed analysis is based on a *calculus of variations theorem* that exploits the *Blade Element-Momentum Theory* with nonlinear aerodynamics and rigorously solves the problem of aerodynamically optimal coaxial rotor.

For aerodynamically optimal rotor, two basic conditions should be fulfilled: (a) the induced velocity distribution should be the one that minimizes the induced power; (b) each cross-section should work in its optimal angle of attack to maximize its ${}^{c_l}/_{c_d}$.

Based on Blade Element Momentum Theory, one may express the thrust and induced power coefficients as:

$$C_T = 4\int_0^1 \tilde{r}\,(\lambda_C+\lambda_i)\,\lambda_i d\tilde{r}, \quad (4a)$$

$$C_{Pi} = 4\int_0^1 \tilde{r}(\lambda_C+\lambda_i)^2\lambda_i d\tilde{r}. \quad (4b)$$

For a given climb velocity distribution, $\lambda_C(\tilde{r})$, the induced power optimization task is focused on the selection of $\lambda_i(\tilde{r})$, that for a given thrust coefficient, C_T, as given by Eq.(4a), will minimize C_{Pi} as given by Eq.(4b). For that purpose we employ the *calculus of variations technique* and adopt the minimization process of an integral of the form

$$J = \int_0^1 F(\tilde{r},\lambda_i,\frac{d\lambda_i}{d\tilde{r}})d\tilde{r},$$

while for the present case of optimization with constraint (minimum induced power for a given thrust) we define:

$$F = C_{Pi}+\eta C_T,$$

where η is a Lagrange multiplier. The above integrand shows that $\lambda_i(\tilde{r})$ should fulfill the following

Euler equation

$$\frac{\partial F}{\partial \lambda_i} = \frac{\partial \left\{ \tilde{r} \left(\lambda_C + \lambda_i\right)^2 \lambda_i + \eta \left[\tilde{r} \left(\lambda_C + \lambda_i\right) \lambda_i\right] \right\}}{\partial \lambda_i} = 0$$

or

$$\tilde{r} \left(\lambda_C^2 + \eta \lambda_C + 4\lambda_C \lambda_i + 2\eta \lambda_i + 3\lambda_i^2\right) = 0. \quad (5)$$

Parasite Power: As far as the parasite power optimization is concerned, each blade cross-section should operate in its optimal effective angle of attack, α_{opt}, where the ratio c_l/c_d is maximal, and, hence, we define $c_l^{opt} = c_l(\alpha_{opt})$, $c_d^{opt} = c_d(c_l^{opt})$.

2.3 The Solution Scheme

In the general case, the above described optimization of a coaxial rotor system is expressed as a nonlinear system of four equations an unknowns, namely:

$$f_i(x_1 \ldots x_4) \quad \text{for} \quad i = 1 \ldots 4$$

where the unknowns are $x_1 = \bar{\lambda}_i^U$ and $x_2 = \bar{\lambda}_i^L$ and $x_3 = \eta^U$ $x_4 = \eta^L$. For a given set of these four values, the following calculations should be executed:

a) Calculate $\lambda_C^U(\tilde{r})$ and $\lambda_C^L(\tilde{r})$ by influence coefficients (or other source).

b) Calculate $\lambda_i^U(\tilde{r})$ and $\lambda_i^L(\tilde{r})$ from the quadratic equation Eq.(5) (applied separately to the upper and lower rotor) as:

$$\lambda_i^X(\tilde{r}) = \frac{1}{3}\left(-A_\lambda + \sqrt{B_\lambda}\right)$$

where

$$A_\lambda = 2\lambda_C^X(\tilde{r}) + \eta^X$$

$$B_\lambda = \left(\lambda_C^X(\tilde{r})\right)^2 + \eta^X \lambda_C^X(\tilde{r}) + \left(\eta^X\right)^2$$

and $X = U, L$.

(c) Calculate the residual functions:

$$\begin{aligned}
f_1 &= C_T - C_T^{TOTAL} \\
f_2 &= C_{Pi}^U + C_{Pd}^U - \left[C_{Pi}^L + C_{Pd}^L\right] \frac{\zeta_R^5}{\zeta_\Omega^2} \\
f_3 &= \bar{\lambda}_i^U - 2\int_0^1 \tilde{r} \lambda_i^U(\tilde{r}) d\tilde{r} \\
f_4 &= \bar{\lambda}_i^L - 2\int_0^1 \tilde{r} \lambda_i^L(\tilde{r}) d\tilde{r}
\end{aligned}$$

Thus, by employing a nonlinear solver, the values of x_i that yield $f_i = 0$ are found.

The simplified case:

In the simplified case, the above optimization problem may be expressed as the following nonlinear algebraic system of nine equations and unknowns:

$$\begin{aligned}
&\left(\lambda_C^U\right)^2 + \eta^U \lambda_C^U + 4\lambda_C^U \lambda_i^U + 2\eta^U \lambda_i^U + 3\left(\lambda_i^U\right)^2 = 0, \\
&\left(\lambda_C^{LI}\right)^2 + \eta^L \lambda_C^{LI} + 4\lambda_C^{LI} \lambda_i^{LI} + 2\eta^L \lambda_i^{LI} + 3\left(\lambda_i^{LI}\right)^2 = 0, \\
&\left(\lambda_C^{LO}\right)^2 + \eta^L \lambda_C^{LO} + 4\lambda_C^{LO} \lambda_i^{LO} + 2\eta^L \lambda_i^{LO} + 3\left(\lambda_i^{LO}\right)^2 = 0, \\
&\lambda_C^U = k^{LU} \left\{ \left(\tilde{r}_w^L\right)^2 \lambda_i^{LI} + \left[1 - \left(\tilde{r}_w^L\right)^2\right] \lambda_i^{LO} \right\} \frac{\zeta_R}{\zeta_\Omega}, \\
&\lambda_C^{LI} = \left[k^{UL} \lambda_i^U\right] \frac{\zeta_\Omega}{\zeta_R}, \\
&C_T^U = 2\left(\lambda_C^U + \lambda_i^U\right) \lambda_i^U, \\
&C_T^L = C_T^{LI} + C_T^{LO}, \\
&C_T^{TOTAL} = C_T^U + C_T^L \frac{\zeta_R^4}{\zeta_\Omega^2}, \\
&C_{Pi}^U + C_{Pd}^U = \left[C_{Pi}^L + C_{Pd}^L\right] \frac{\zeta_R^5}{\zeta_\Omega^2},
\end{aligned} \quad (6)$$

where the unknowns are

$$C_T^U, C_T^L, \lambda_C^U, \lambda_C^{LI}, \lambda_C^{LO}, \lambda_i^U, \lambda_i^{LI}, \lambda_i^{LO}, \eta^U, \eta^L,$$

and $\lambda_C^{LO} = 0$ in hover case.

Note that C_T^{TOTAL} represents the total required trust and that the last equation of Eqs.(6) stands for the torque balance condition which is required in a coaxial system.

The coaxial rotor optimal design obtained is shown in Fig. 3 for the simplified case and in Fig. 4 for the general case; unlike the single rotor optimal design, the inflow is not uniform and the chord and the twist decrease with r but not exactly.

3 Rigid wake model

3.1 Single rotor analysis

To derive this model, it is assumed that the blade advances at each time step Δt by an angle

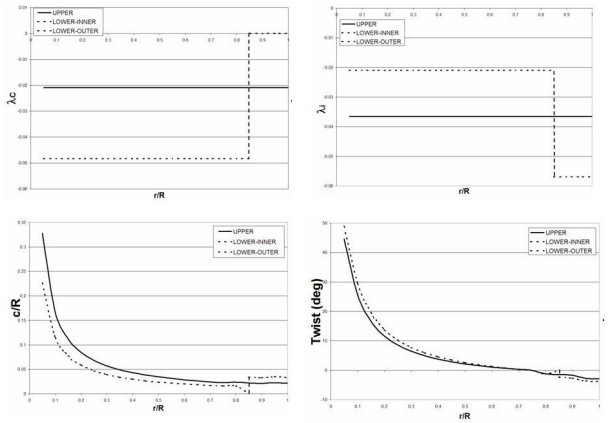

Fig. 3 Optimal design of a coaxial rotor, simplified case;

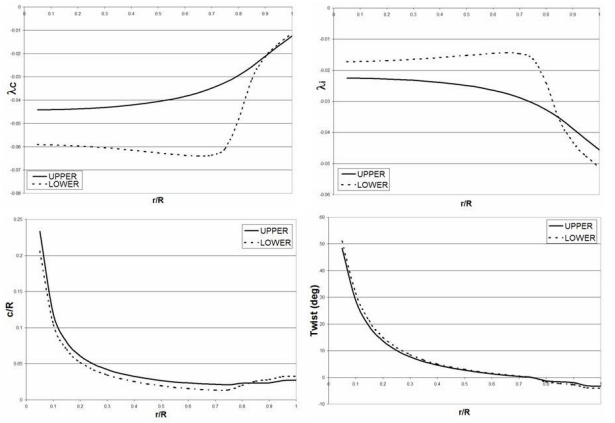

Fig. 4 Optimal design of a coaxial rotor, general case;

$\Delta\Psi$ equals to: $\Delta\Psi = \Omega\Delta t$. At each time step, a vortex point is created and the vortex points created before are convected downwards and radially inward below the rotor with the vertical distance $\Delta\tilde{z} = \tilde{v}_{iz}\Delta\Psi$ and radial distance $\Delta\tilde{r} = \tilde{v}_{ir}\Delta\Psi$ while $\tilde{v}_{iz}$ and $\tilde{v}_{ir}$ are axial and radial induced velocities (see Fig. 5).

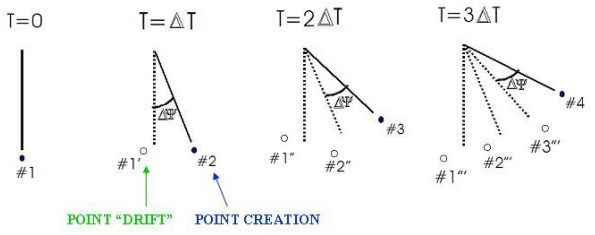

Fig. 5 Time-marching scheme.

Each existing vortex point trailing from each blade is moving in the radial and axial directions during a small increment of time Δt thanks to the following relations:

$$\begin{cases} r_{t+\Delta t} = r_t + v_{\mathrm{ir}}\Delta \mathrm{t} \\ z_{t+\Delta t} = z_t + v_{iz}\Delta \mathrm{t} \end{cases} \tag{7}$$

where v_{ir} and v_{iz} are induced velocities function of the vertical position z of the vortex point and defined here after:

$$\begin{cases} \tilde{v}_{iz} = \dfrac{\lambda_0}{\Lambda(z)} \\ \tilde{v}_{ir} = \dfrac{dr(z)}{dz}\cdot\tilde{v}_{iz} = -\dfrac{R\cdot c_f\cdot\lambda_0}{2}[\Lambda(z)]^{-\frac{3}{2}}\left(\Lambda(z) - \dfrac{A_\infty}{A_0}\right) \end{cases} \tag{8}$$

where λ_0 is the mean induced inflow over the disk that may be given by General Momentum Theory, $\Lambda(z)$ the ratio of cross-sectional area (or inflow) to that at the rotor level. $\frac{A_\infty}{A_0}$ is the ratio of cross-sectional area infinite downstream to rotor disk area and c_f is a contraction factor that are obtained from experiments. Moreover, the tip vortex radial displacement has been approximated by an exponential decay, based on experimental and computational collected data from the open literature.

The process is repeated for each blade and is performed until a complete wake structure is obtained.

Physical arguments show that the rigid wake geometry must be consistent, i.e the induced inflow used to generate the wake (λ_0) must match with the induced inflow of the resulting wake (calculated by Biot-savart, on the blade). Therefore an iterative loop on the induced inflow (average over the disk) is performed until convergence. Moreover, a loop on the pitch is achieved in order to find the pitch angle that provides the required thrust.

As shown in Fig. 6, the trajectory formed by the tip vortex of one blade traces out a contracted helix form with a distance between two spires that increases as the wake goes down and the contraction is practically complete within only about half a rotor radius. Nevertheless, a steady and well defined wake does not really exist beyond about four revolutions due to dissipation and as

mentioned before the spatial location of the tip vortices is dependent of the modeling parameter values selected (c_f and $\frac{A_\infty}{A_0}$).

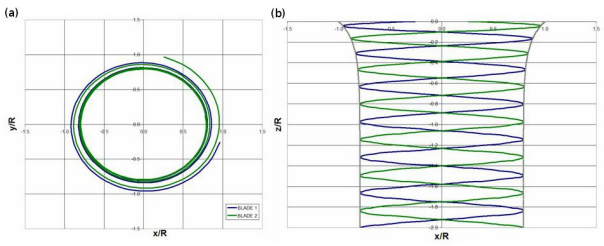

Fig. 6 Single rotor rigid wake;(a) top view, (b) side view; c_f= 5, $\frac{A_\infty}{A_0} = 0.6$, $N_b = 4$, $C_T = 0.004$, $\theta_{tw} = 13°$.

3.2 Coaxial rotor analysis

The rigid wake of the coaxial rotor is built similar to the rigid wake of the single rotor. First, the rigid wakes of two isolated rotors are built, separated by a clearance of $0.2R$. Then, the inflow from the two wakes over each rotor disk is calculated, each wake with his own circulation. The inflow from the two wakes is computed on each rotor disk in order to take into account the interactions between the two rotors and then it's used to create again the wakes of each rotor until consistency (inflow convergence) of the coaxial rotor wake is obtained. There is also a loop on the collective pitch angles that insures the torque balance and that the total thrust is equals to the thrust required.

4 Free wake model

4.1 Single rotor analysis

In this approach, no preconceived assumption is made regarding the wake form and no experimental results are required for formulation purposes. The wake is free to assume any shape that may result from the mutual interaction between the total vortex system of the rotor and the velocity field induced by this system; the position vectors of the individual wake filaments are now part of the solution process.

The free wake model developed in this study is based on the type-marching method with an explicit numerical scheme. The free wake construction starts by an initial rigid wake geometry: only two vortex filaments are sufficient. At each time step Δt, the blade rotates through an azimuthal increment, $\Delta\psi$, a new vortex point is created and the vortex elements not attached to the blades are modified in turn to conform with the induced velocity field (see Fig. 5).

Using the Biot-Savart law which includes a core growth (vorticity diffusion) model, the induced velocity field of the total vortex system is computed at each vortex element where the curved vortex filaments are approximated by straight-line vortex segments. The convection of the vortex points follows an explicit numerical scheme such as :

$$\begin{cases} x_{t+\Delta t} = x_t + v_{\mathrm{ix}} \cdot \Delta \mathrm{t} \\ \mathrm{y}_{t+\Delta t} = y_t + v_{iy} \cdot \Delta \mathrm{t} \\ z_{t+\Delta t} = z_t + v_{iz} \cdot \Delta \mathrm{t} \end{cases} \tag{9}$$

where v_{ix}, v_{iy}, v_{iz} are induced velocity field components that are calculated (thanks to Biot-Savart law) at each vortex point at each time step by all tip vortices of all blades of all wakes.

The process is allowed to iterate until satisfactory convergence has been achieved, which means that the transients introduced by the initial condition die out and a periodic solution is achieved (steady state).

As mentioned before, the free wake is built thanks to the induced velocity calculated on the tip vortex itself and this induced velocity depends linearly on the circulation. Like the lift, the circulation presents a maximum at the tip region. Therefore, the maximum circulation has been used to generate the free wake and an iterative loop on this maximal circulation has been performed in order to get a consistent wake. Moreover, a loop on the pitch is achieved in order to find the pitch angle that provides the required thrust.

As shown in Fig. 7, the trajectory formed by the tip vortex of one blade traces out a contracted helix form with a distance between two spires that increases as the wake is moving down.

Moreover, the free wake generated shows that a steady and well defined wake does not really exist beyond about four revolutions and that the contraction is practically complete within only about half a rotor radius. Furthermore, only the free wake model allows modeling the roll-up of the tip vortices. Finally, the tip vortices roll-up convect downstream and grow due to diffusion with the time (see Fig. 8), phenomenon also observed during experiments (Ref [2]) or in CFD (Ref [3]).

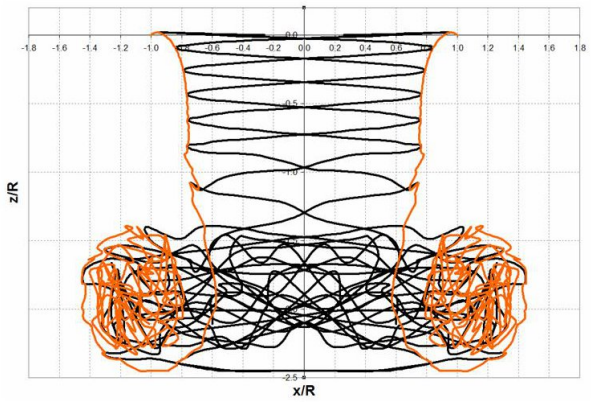

Fig. 7 Single rotor free wake. $N_b = 4$, $C_T = 0.004$, $\theta_{tw} = 13°$.

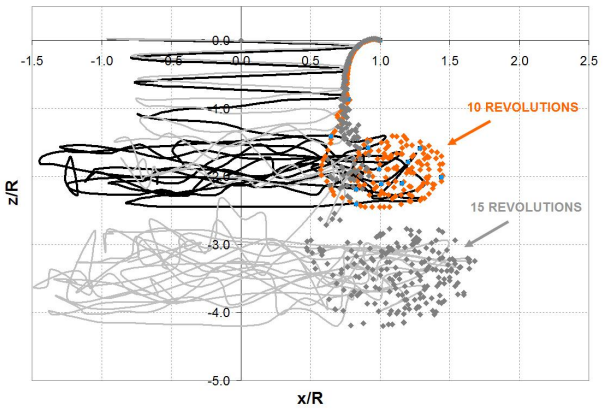

Fig. 8 Roll up of the tip vortices for two free wakes of 10 and 15 revolutions. $N_b = 4$, $C_T = 0.004$, $\theta_{tw} = 13°$.

The present methodology requires to add a vortex point at each time step. With the time the number of vortex points might become important and the ones creating at the beginning of the process may not participating to the velocity field due to diffusion. A solution to this problem is to throw out the oldest vortex point each time a new one is created.

Once the free wake was built, the inflow of the wake was calculated over the rotor disk plan as presented in Fig. 9. The inflow is azimuthally uniform. Moreover, it is constant and very close to the inflow given by the General Momentum Theory for about $r/R < 0.8$. The irregular distribution of the inflow at the outboard region is due to the presence of the tip vortex. Furthermore, the tip vortex position above the blade gives an upwash at the tip region of the rotor disk. Finally, there is a good correlation of the inflow distribution towards the tip with the experimental one of Ref [1]: the small increase, the sharp decrease and the upwash at the tip are at the right place and at the right magnitude. Due to measurement difficulties, the experimental inflow distribution inboard is not valid and therefore not comparable.

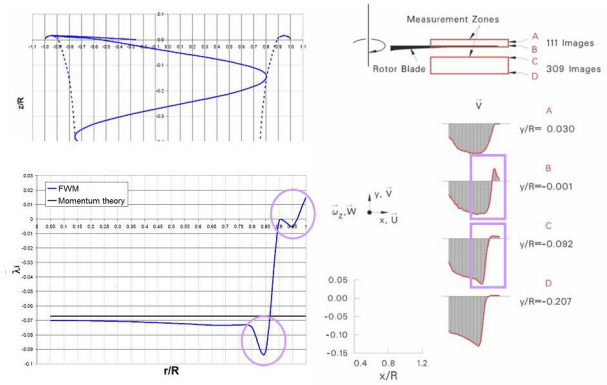

Fig. 9 Inflow distribution of single rotor free wake. $N_b = 3$, $C_T = 0.009$, $\theta_{tw} = 13°$.

4.2 Coaxial rotor analysis

The free wake of the coaxial rotor is built similar to the free wake of the single rotor; the solution scheme implemented is presented in Fig. 10. The free wakes of each rotor are built simultaneously: each vortex point is moving by the induced velocity of the two wakes (all the vortex filaments trailed from each blade of each rotor), the maximal circulation of each wake being considered. Once the two free wakes are built, the

induced velocity from the two wakes (with their own constant circulation) over each rotor disk is calculated in order to calculate the loads of each rotor. The maximum of the circulation (through Biot-Savart law) is then used to create again the free wakes until convergence of the maximum circulation is obtained for each wake (consistent wake). Moreover, there is a loop on the pitch angles to ensure the torque balance and that the total thrust is equals to the thrust required.

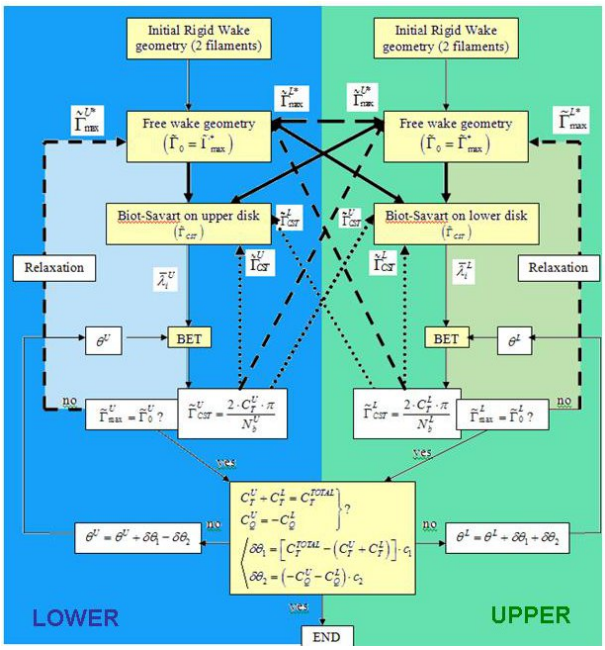

Fig. 10 Solution scheme for coaxial rotor free wake.

Fig. 11 shows the coaxial rotor free wake obtained and Fig. 12 its roll up tip vortices convection and the diffusion with the time. Like in the single rotor analysis, the free wake model allows a good modeling of the coaxial rotor tip vortices roll up and their convection downstream with time until dissipation.

Fig. 13 presents the tip vortices axial and radial displacements. Well correlated with experiments and CFD of Ref [3], the upper rotor wake is more stretched and more contracted than the lower rotor wake.

As shown on Fig. 14, the inflow distribution is relatively uniform over the two rotor disks: the inflow decreases smoothly towards the tip on the upper rotor disk whereas it decreases sharply on the lower rotor disk and there is also an upwash at the tip of the lower disk. Compared with the experiments of Ref [1], the free wake modeling provides a good correlation of the outboard inflow distribution at each rotor disk, and surprisingly the analytical point of view allows a reasonable prediction as well.

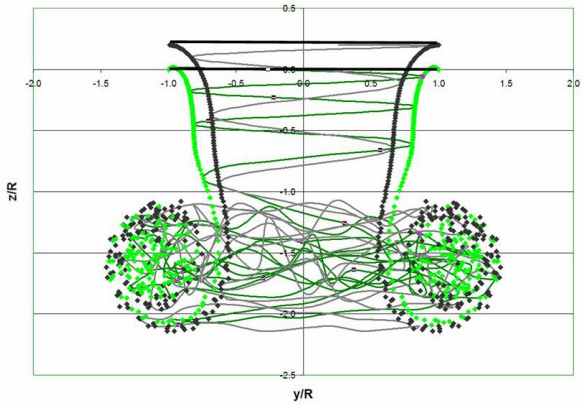

Fig. 11 Free wake of a coaxial rotor; $N_b^L = N_b^U = 4$, $C_T = 0.004$, $\theta_{tw} = 13°$.

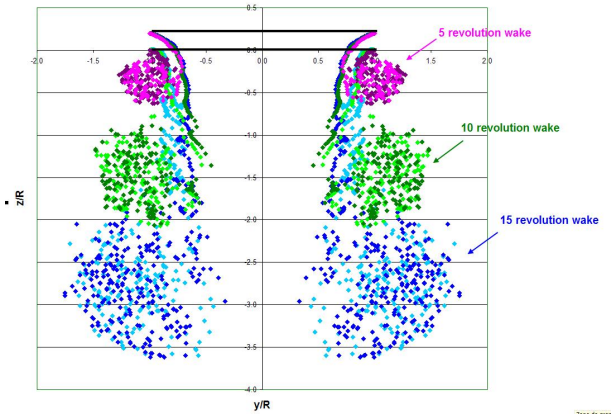

Fig. 12 Free wake contraction boundaries, roll up of the tip vortices, convection and diffusion for a coaxial rotor; $N_b^L = N_b^U = 4$, $C_T = 0.004$, $\theta_{tw} = 13°$.

5 Comparative study

A comparison between the three points of views has been performed on the pitch angle and the inflow distributions (see Fig. 15). The analytical and free wake points of view provide close

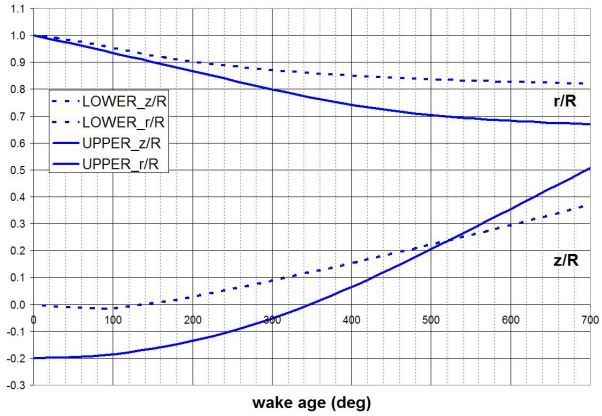

Fig. 13 Tip vortices axial and radial displacements of coaxial rotor free wake; $N_b^L = N_b^U = 4$, $C_T = 0.004$, $\theta_{tw} = 13°$.

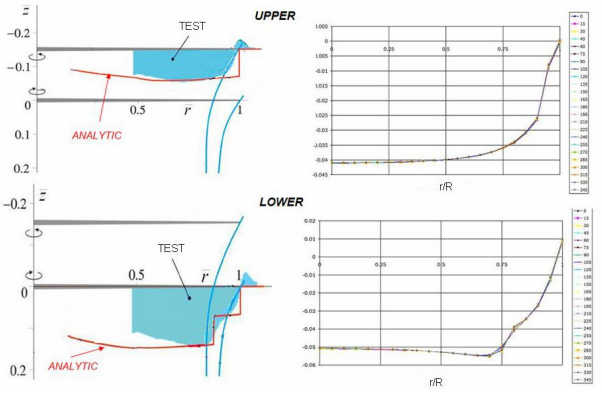

Fig. 14 Inflow distribution comparison with Ref [1].

results that have been well correlated with experiments. However, some differences with the rigid wake model may be explained by the simplicity and poor physical justification of the model employed.

6 Advantages and disadvantages of each formulation

It is important to underline the advantages and disadvantages of each formulation, see also Fig. 16.

The analytical approach does not require any experimental or test data. Its computational cost for preliminary design and simulation is negligible. However, this approach does not allow a wake modeling. Yet, surprisingly, a reasonable prediction of the average inflow of the wake is

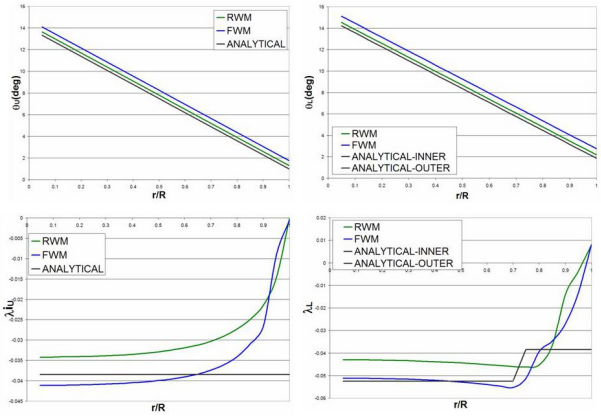

Fig. 15 Pitch and inflow distribution from the 3 points of view. (left):upper disk, (right):lower disk .$N_b^L = N_b^U = 4$, $C_T = 0.004$, $\theta_{tw} = 13°$.

offered by this approach. Compared with the numerical prediction models, the optimization enabling is of very important quality in this approach.

The rigid wake approach requires a intermediate computational cost. However, this method uses experimental data to locate the tip vortex position of a simplified rigid wake; the limitation of the wake geometry prediction is therefore not suitable for interactional aerodynamic. Moreover, the physical justification is very poor and an optimization process using this method is time consuming.

The free wake approach is based on a very good physical foundation and allows generating a detailed wake modeling: more wake effects are present like the roll-up of the tip vortices or the absent of a steady and well defined wake after few revolutions (diffusion). The wake modeling is very close to the experimental one in terms of geometry and inflow distribution. Moreover, this approach does not require any experimental or test data. However, a high computational cost is required for preliminary design and simulation (still negligible compared to CFD computational cost). Optimization process using this method is lengthy and not feasible.

	Analytical	RWM	FWM
Computational cost (PD & simulation)	negligible	medium	high
Requirement of experimental data	no	yes	no
Wake modeling quality	no wake	Simplified (not suitable for interactional aero).	detailed/ similar to experiments
Inflow distribution prediction	reasonable	approximate	good
Optimization Enabling	Very Good	Lengthy	Extremely lengthy
Physical Justification	Reasonable	poor	Very Good

Fig. 16 Summary of the advantages and disadvantages of the three discussed methods.

7 Conclusion

Generic coaxial rotor systems in hover were analyzed in a uniform level by three different approaches.

The analytical point of view enabled a new optimized solution that may also be refined using numerical/experimental data. Optimization shows that unlike the classical single rotor optimization, the induced velocity in an optimized coaxial rotor system is not uniform and the chord and the twist distribution generally decrease with r but not exactly. Furthermore, analytic solution shows surprisingly good agreement with experiments.

Rigid wake analysis lakes some of the insight provided by the analytic solution and reveal only limited wake effects. It is also very sensitive to its modeling parameters.

Free wake analysis provides good quality wake modeling, reasonably predicts the downwash and hence the performance of a coaxial system. Moreover, free wake models enable the determination of the rotor influence on other parts of the airframe. Finally, free wake models are not suitable for real time simulation-type analysis and optimization due to high computational cost.

Therefore, the best approach to the analysis of coaxial rotor configurations is depending on the objective: the analytical approach will be more adapted for a design optimization or quick estimation of coaxial rotor performance (for simulation and preliminary design) whereas the free wake model will be selected for the influence of the coaxial rotor wake on others parts of the airframe or for a more accurate prediction of the coaxial rotor performance that may be incorporated in trim analysis and vast preliminary parametric studies. On the other side, the rigid wake model developed should not be considered as a true predictive method. As a general conclusion, the analytical and free wake model approaches presented in this study are complementary tools for the development of a coaxial rotor helicopter.

References

[1] McAlister, Tung, *Experimental study of a hovering coaxial rotor with highly twisted blades*. American Helicopter Society 64th Annual Forum, 2008.

[2] Landgrebe A.J *The wake geometry of a hovering helicopter rotor and its influence on rotor performance*. Journal of the American Helicopter, Vol.17, No.4 1972.

[3] Richard E Brown, Hyo Won Kim *A comparison of coaxial and conventional rotor performance*. American Helicopter Society 62nd Annual Forum, 2006.

Copyright Statement